Potentiality of Metal-Oxide-Semiconductor Silicon Optical Modulator Based on Free Carrier Absorption

Tetsuo Tabei*, Tomoki Hirata†, Kenta Kajikawa‡, and Hideo Sunami

Research Institute for Nanodevice and Bio Systems, Hiroshima University,

Higashihiroshima, Hiroshima 739-8527, Japan

Light propagation in a metal-oxide-semiconductor optical modulator based on free carrier absorption is analyzed theoretically. The analysis is based on Marcatili's approximation taking account of absorption by free carriers in the inversion layer. The gate voltage and wavelength dependences of propagation loss and extinction ratio are also evaluated. The free carrier absorption in the proposed modulator is appropriately confirmed by comparing theoretical results with the experimental result of fabricated optical modulators on silicon-on-insulator wafers; however, practical use of the device is limited since the extinction ratio remains small owing to a weak interaction between light and inversion carriers at 1.55-μm-wavelength light. By theoretical analyses, a large extinction ratio is obtained for possible applications in the deeper infrared regime because free carrier absorption increases with wavelength. A much larger extinction ratio is expected when the interaction between guided waves and surface plasmons occurs.

* E-mail address: tabei@hiroshima-u.ac.jp
† Present address: Sagamihara Plant, Nikon Corporation, Sagamihara, Kanagawa 228-0828, Japan.
‡ Present address: OMRON Corporation, Kyoto 600-8530, Japan.

1. Introduction

To cope with signal propagation delay in metal wiring in large-scale integrated circuits, on-chip optical interconnect has long been proposed owing to its inherent features such as the absence of resistance-capacitance time delay, cross-coupled structure, and multiple-signal transfer. To realize optical interconnect, silicon optical modulators such as p-i-n diodes based on free carrier absorption[1)], Mach-Zehnder-type metal-oxide-semiconductor (MOS) capacitors[2, 3)] or p-n diodes[4)] based on phase shift, bipolar mode transistors based on free carrier absorption[5)], and ring resonators[6)] have been proposed.

On the other hand, the authors have proposed a comb-shaped MOS capacitor optical modulator based on free carrier absorption[7)]. The optical modulator based on free carrier absorption has a strong potential for multiwavelength propagation due to its desirable insensitivity to wavelength compared with a phase-shift-based modulator. The proposed device has high compatibility with conventional MOS device structures and potential applications in deep infrared optical modulators. Light modulation by our proposed modulator was confirmed experimentally and reported in ref. 8. In this report, we will describe the light propagation characteristics of our proposed device and confirm optical modulation based on free carrier absorption by theoretical analyses. Furthermore, the potentiality of the silicon optical modulator based on free carrier absorption will be discussed.

2. Basic Idea

The modulation mechanism of our proposed modulator is based on the absorption by free carriers.[10-12)] The light absorption coefficient of a material is given by $4\pi\,\mathrm{Im}(n)/\lambda$, where n is the complex refractive index that is related to the dielectric function ε by $n = \varepsilon^{1/2}$, and λ is the optical wavelength. The dispersion of the dielectric function by free carriers is described by the classical

Drude model as follows:

$$\varepsilon = \varepsilon_\infty - \frac{N_c e^2}{m_c \varepsilon_0 (\omega^2 + i\omega/\tau_c)}, \tag{1}$$

where N_c, m_c, and τ_c are the concentration, effective mass, and relaxation time of free carriers, respectively. e and ε_0 are the elementary charge and permittivity in vacuum, respectively. ε_∞ denotes the contribution from polarization except for free carriers and ω is the angular frequency of light ($\omega = 2\pi c/\lambda$, c is light speed). i is the imaginary unit. Figure 1 shows the wavelength dependence of the absorption coefficient of impurity-doped crystalline silicon. The free carrier concentration N_c is set to $N_c = N_A$ or $N_c = N_D$, where N_A and N_D denote impurity concentrations of the acceptor and donor, respectively. The value of ε_∞ is set to 11.9. The relaxation times of holes in boron-doped crystalline silicon, τ_h, and electrons in phosphorus-doped crystalline silicon, τ_e, are set as follows:

$$\begin{aligned} \tau_h &= \frac{0.34 m_0}{e}\left[61.8 + \frac{8.21\times10^{10}}{(N_A + 3.58\times10^{16})^{1/2}}\right], \\ \tau_e &= \frac{0.33 m_0}{e}\left[3.07 + \frac{2.88\times10^{11}}{(N_D + 3.98\times10^{16})^{1/2}}\right], \end{aligned} \tag{2}$$

where m_0 is the electron rest mass. The above function form is fitted to the data of mobility quoted from ref. 13, and the values of m_c for free carriers in impurity-doped crystalline silicon are referred to ref. 14. As shown in Fig. 1, absorption coefficient increases when the optical wavelength or the free carrier concentration becomes large. Thus, the power of light propagating in silicon can be changed when the free carrier concentration is controlled. In the following section, 1.55 μm wavelength is chiefly analyzed because it is widely used for optical interconnect even though a higher extinction ratio is obtained in the case of a larger wavelength, as expected from Fig. 1. The case of a larger wavelength is discussed in §3.3 and 3.4.

The light modulator proposed in this study has an MOS structure, as shown in Fig. 2(a). The waveguide core is silicon-on-insulator (SOI), and the underlying clad layer is buried oxide. The side and

upper clad layers are thin SiO_2 films, and an impurity-doped polycrystalline silicon that functions as a gate electrode covers it. The modulation mechanism is shown in Fig. 2(b). The input light propagates inside SOI repeating reflections. When the inversion layer (or accumulation layer) with high-concentration free carriers is formed by applying a large bias voltage to the gate electrode, the reflectivity at the interface of the core and the clad decreases owing to free carrier absorption. As a result, the power of output light decreases.

3. Theoretical Analysis

3.1 Calculation method

Only the absorption by the inversion layer is discussed here neglecting behavior under accumulation condition. For simplicity, the motion of carriers in the inversion layer is treated classical mechanically even though it must be treated quantum mechanically because carriers are confined in a narrow region of 1-10 nm from the Si/SiO_2 interface. In the following, SOI is assumed to be p-type silicon that is doped with boron of $N_A = 1.5 \times 10^{15}$ cm^{-3}.

The free carrier concentration n_I of the inversion layer at the Si/SiO_2 interface is given by $n_I = n_i^2 \exp(e\phi_s/k_BT)/N_A$, where n_i is the intrinsic carrier concentration, ϕ_s is the surface potential at the Si/SiO_2 interface, k_B is the Boltzmann constant, and T is the temperature. Inversion layer thickness is calculated as $-Q_I/en_I$, where Q_I is the charge concentration per unit area of the inversion layer, which is derived from Poisson's equation. In the case of a strong inversion, Q_I is written as

$$Q_I = -\sqrt{2\varepsilon_{Si}\varepsilon_0 k_B T n_i^2 / N_A}\, e^{e\phi_s/2k_BT} . \quad (3)$$

The mobility of free electrons in the inversion layer is set to $\mu_{eff} = e\tau/m_e \approx 32500\, E_{eff}^{-1/3}$ [15], where E_{eff} denotes the effective normal field $E_{eff} = (|Q_D|+|Q_I|/2)/(\varepsilon_{Si}\cdot\varepsilon_0)$, Q_D is the charge concentration per unit area of the depletion layer, and ε_{Si} is the dielectric constant of silicon. The above expression is adopted for

μ_{eff} even though this expression does not hold for large E_{eff} owing to surface roughness. For simplicity, electron effective mass is set to $m_{\mathrm{e}} = 0.26\ m_0$[14] for nondoped crystalline silicon, which is obtained from the mean curvature of the electron energy band $E(\boldsymbol{k})$ [$\boldsymbol{k} = (k_1, k_2, k_3)$ is the electron wave vector] using

$$\frac{\hbar^2}{m_{\mathrm{e}}} = \frac{1}{3}\sum_{i=1}^{3}\frac{\partial^2 E(\boldsymbol{k})}{\partial k_i \partial k_i} = \frac{\hbar^2}{3}\left(\frac{2}{m_{\mathrm{t}}} + \frac{1}{m_{\mathrm{l}}}\right), \tag{4}$$

at the extreme point $\partial E(\boldsymbol{k})/\partial k_i = 0$, where m_{t} (= 0.19 m_0) and m_{l} (= 0.98 m_0) are the transverse and longitudinal effective masses, respectively.

As all physical quantities in terms of the inversion layer are expressed as a function of the surface potential ϕ_{s}, the relation with the gate voltage $V_{\mathrm{G}} = \phi_{\mathrm{s}} - Q_{\mathrm{T}}/C_0$ can be investigated through the parameter ϕ_{s}, where Q_{T} and C_0 denote the total charge concentration per unit area and the capacitance of the gate oxide film, respectively. Flat band voltage is neglected for simplicity. We used *Mathematica* for simulations. Figure 3 shows the real part of the dielectric function Re(ε) and the absorption coefficient of the inversion layer in p-type silicon when gate voltage is applied. When the real part of the dielectric function Re(ε) becomes less than 0, the inversion layer behaves like metal and absorption coefficient increases rapidly. The gate voltage dependence of reflectivity for transverse electric (TE) and transverse magnetic (TM) polarized plane waves entering from SOI to the clad layer is shown in Fig. 4. The refractive index of each material for λ = 1.55 μm is also denoted. For simplicity, the imaginary parts of the refractive index of silicon and SiO_2 are ignored because they are very small. Also, the depletion layer in SOI and the depletion or accumulation layer in polysilicon are neglected. The incident angle of a plane wave is set to 82.6° for TE polarization and 89.7° for TM polarization. (These angles are obtained by the wave vector of the $E_{11}^{\ y}$ mode for a waveguide of 1.5 μm thickness and 50 μm width, which will be discussed later.) The attenuation of optical power is very small by one reflection because the inversion layer is very thin. The sharp decrease in reflectivity obserbed for TM polarized waves is due to absorption by the surface plasmon.[16] When the applied gate voltage is increased, the

reflectivity of both TE and TM polarized waves slowly decreases. However, this value is limited because the dielectric breakdown occurs when applying a large electric field, which is about 10 MV/cm, to the gate oxide film.

To investigate the light propagation characteristics, Marcatili's method[17] is utilized. The core and clad are set, as shown in Fig. 5, where polysilicon and the buried oxide layer are assumed to be infinite half-plane, while the thin SiO_2 layer (gate oxide) and shaded regions are ignored for simplicity. The propagation light in a waveguide is decomposed to the guided modes E_{pq}^{x} and E_{pq}^{y}, which have the main component of electric field in the x and y directions, respectively. Each guided mode is expressed as the superposition of plane waves characterized by the wave vector $\boldsymbol{k}_{pq} = (k_{xp}, k_{yq}, \beta_{pq})$, and its components are given by

$$\begin{aligned} k_{ip} &= \frac{2\pi}{\lambda}\sqrt{\left(n_{\mathrm{Si}}^2 - n_{\text{Poly-Si}}^2\right)\left(1-\nu_{ip}\right)} \quad (i = x, y), \\ \beta_{pq} &= \sqrt{\frac{4\pi^2 n_{\mathrm{Si}}^2}{\lambda^2} - k_{xp}^2 - k_{yq}^2}\,, \end{aligned} \tag{5}$$

where each ν_{ip} satisfies the following equation[17]

$$\begin{aligned} &\frac{2\pi T_{\text{core}}}{\lambda}\sqrt{\left(n_{\mathrm{Si}}^2 - n_{\text{Poly-Si}}^2\right)\left(1-\nu_{xp}\right)} - \tan^{-1}\sqrt{\gamma_1\frac{\nu_{xp}}{1-\nu_{xp}}} \\ &\quad - \tan^{-1}\sqrt{\frac{\gamma_2}{1-\nu_{xp}}\left(\frac{n_{\text{Poly-Si}}^2 - n_{\mathrm{SiO2}}^2}{n_{\mathrm{Si}}^2 - n_{\text{Poly-Si}}^2} + \nu_{xp}\right)} = (p-1)\pi \quad (p = 1, 2, \ldots), \\ &\frac{2\pi W_{\text{core}}}{\lambda}\sqrt{\left(n_{\mathrm{Si}}^2 - n_{\text{Poly-Si}}^2\right)\left(1-\nu_{yq}\right)} - 2\tan^{-1}\sqrt{\gamma_3\frac{\nu_{yq}}{1-\nu_{yq}}} = (q-1)\pi \quad (q = 1, 2, \ldots), \end{aligned} \tag{6}$$

with $\gamma_1 = n_{\mathrm{Si}}^2 / n_{\text{Poly-Si}}^2$, $\gamma_2 = n_{\mathrm{Si}}^2 / n_{\mathrm{SiO_2}}^2$, and $\gamma_3 = 1$ for the E_{pq}^{x} mode, and $\gamma_1 = \gamma_2 = 1$ and $\gamma_3 = n_{\mathrm{Si}}^2 / n_{\text{Poly-Si}}^2$ for the E_{pq}^{y} mode. The integers p and q denote the number of extremes of the x and y directions, respectively, and these label guided modes. Figure 6 shows examples of field distribution plots of the E_{11}^{y}, E_{21}^{y}, and E_{31}^{y} modes obtained by Marcatili's approximation. Though free carrier absorption is not considered yet here, the propagation loss by polysilicon appears. The propagation loss is larger when

the mode is of the higher order.

To investigate the gate voltage dependence of the light modulation of the proposed modulator, we must consider the clad layer with a multilayer structure, as shown in Fig. 4(a). Owing to the difficulty in the accurate calculation of the gate voltage dependence based on Marcatili's approximation, a simplified method is used as follows. For example, when reflectivity is given by R, the power after n-times reflection is $P_0R^n = P_0 \exp[-n \ln(1/R)] = P_0 \exp[-z\,(n/z) \ln(1/R)]$ as the initial power P_0 and propagation length z. Thus, the loss coefficient a is given by $a = (n/z) \ln(1/R)$. In the case of a rectangular waveguide, the light power after propagation of length z can be expressed as $P_{pq}(z) = P_0\exp[-a_{pq}\,z]$ with

$$a_{pq} = -\frac{\ln(R_1R_2)}{L_{xpq}} - \frac{\ln(R_3R_4)}{L_{ypq}}, \tag{7}$$

where

$$\begin{aligned} L_{xpq} &= \frac{2(T_{\text{core}} + \Lambda_{1p} + \Lambda_{2p})\,\mathrm{Re}(\beta_{pq})}{\mathrm{Re}(k_{xp})}, \\ L_{ypq} &= \frac{2(W_{\text{core}} + \Lambda_{3p} + \Lambda_{4p})\,\mathrm{Re}(\beta_{pq})}{\mathrm{Re}(k_{yq})}. \end{aligned} \tag{8}$$

R_i is the reflectivity at the interface S_i, as shown in Fig. 7. Λ_{ip} denotes the penetration depth of an evanescent wave at S_i,

$$\begin{aligned} \Lambda_{1p} &= \left\{\mathrm{Re}\left[\frac{2\pi}{\lambda}\sqrt{(n_{\text{Si}}^2 - n_{\text{Poly-Si}}^2)\nu_{xp}}\right]\right\}^{-1}, \\ \Lambda_{2p} &= \left\{\mathrm{Re}\left[\frac{2\pi}{\lambda}\sqrt{(n_{\text{Si}}^2 - n_{\text{Poly-Si}}^2)\left(\nu_{xp} - \frac{n_{\text{Poly-Si}}^2 - n_{\text{SiO}_2}^2}{n_{\text{Si}}^2 - n_{\text{Poly-Si}}^2}\right)}\right]\right\}^{-1} \\ \Lambda_{3q} &= \Lambda_{4q} = \left\{\mathrm{Re}\left[\frac{2\pi}{\lambda}\sqrt{(n_{\text{Si}}^2 - n_{\text{Poly-Si}}^2)\nu_{yq}}\right]\right\}^{-1}. \end{aligned} \tag{9}$$

The propagation loss α_{pq} is given by $\alpha_{pq} = 10 \log_{10}[P_{pq}(z)/P_0]/z = 10a_{pq}/\ln 10$. Assuming that the real parts of the component of the wave vector, namely, $\mathrm{Re}(k_{xp})$, $\mathrm{Re}(k_{yq})$, and $\mathrm{Re}(\beta_{pq})$, do not change after the inversion layer appears, the propagation loss by free carrier absorption can be obtained by substituting

reflectivity, as shown in Fig. 4, in eq. (7). For the E_{pq}^{y} mode, the light entering into S_1 or S_2 is considered to be a TE polarized wave, and the light entering into S_3 or S_4 is a TM-polarized wave. For the E_{pq}^{x} mode, TE and TM are exchanged. The incident angle of a plane wave is determined by Re(k_{xp}), Re(k_{yq}), and Re(β_{pq}).

3.2 Light modulation for wavelength $\lambda = 1.55$ μm

The propagation loss $\alpha(V_G)$ of the E_{11}^{y} mode with the applied voltage V_G for the modulator of 1.5 μm thickness and 50 μm width is shown in Fig. 8(a). There is energy loss caused by polysilicon absorption, and it becomes large when the gate oxide film becomes thin because the penetration depth of the evanescent wave becomes large. With increasing applied gate voltage, the propagation loss becomes large owing to inversion carrier absorption. Figure 8(b) shows the extinction ratio of the E_{11}^{y} mode for this modulator of 5 mm length. The extinction ratio is given by $10\log_{10}(P_{on}/P_{off})$ and is also expressed as $|\alpha(V_G) - \alpha(0)|\, z$, where P_{off} or P_{on} expresses the light power when gate voltage is applied (light power is small) or not (light power is large). A higher extinction ratio is obtained by applying a higher gate voltage, but it is limited by the dielectric breakdown of the gate oxide film.

Figure 9 shows the propagation loss and the extinction ratio of the E_{11}^{x} mode with applied voltage for the modulator of the same size as mentioned above. The behaviors of gate voltage dependence are similar to those in the case of the E_{11}^{y} mode, but sharp increase appears owing to surface plasmon absorption. In the case of the E_{11}^{y} mode of the present waveguide size, a large absorption by surface plasmons does not appear. Because this waveguide width is very large compared with wavelength, the incident angle of the TM polarized wave entering the side wall of the waveguide is nearly 90°. Thus, the reflectivity of the TM polarized wave at the side wall is nearly 1.

Figure 10 shows the optical responses of the fabricated modulator reported in ref. 8 and theoretical

plots of guided modes. P_{on} of the theoretical plot is set to the value at the gate voltage -1 V. (Flat band voltage is set to -1 V from the observed capacitance-voltage curve of the fabricated device in ref. 8.) For this modulator, the guided modes E_{pq}^{y} of p = 1, 2, and 3 and q = 1, 2, ···, and 98 exist. Even though the optical response is very small, the free carrier absorption in this device is confirmed by the theoretical and experimental analyses. The experimental data fit the most to the theoretical curves of the E_{1q}^{x} or E_{1q}^{y} mode (q = 1, 2, ···) among the various modes. Therefore, the E_{1q}^{x} and E_{1q}^{y} modes whose propagation losses are smaller than those of other E_{pq}^{x} and E_{pq}^{y} modes (p = 2, 3, q = 1, 2, ···) may be dominant in the fabricated optical modulator described in ref. 8.

3.3 Analyses of wavelength dependence

Figures 11(a) and 11(b) show the extinction ratios of the modulator of the same size as mentioned in the previous subsection in the case of wavelength λ = 3 or 5 μm. The refractive indices of SOI and SiO_2 are given by the curve in Fig. 11(c), which is fitted to the data quoted from ref. 18, and a large extinction coefficient of SiO_2 at about λ = 9 μm is neglected. For simplicity, the refractive index of impurity-doped polysilicon is used at the same value as that in the case of λ = 1.55 μm. As mentioned in §2, large extinction ratios are obtained in the case of a large wavelength. However, the extinction ratios are limited owing to the waveguide structure. Since the proposed modulator has an asymmetric structure in the vertical direction, the cutoff wavelength λ_{cut} of the fundamental mode exists. Figure 11(d) shows the wavelength dependence of extinction ratio with the applied gate voltage V_G = 5 V for the modulator of 50 μm width, 5 mm length, and 0.3, 0.5, 1, or 1.5 μm thickness. The cutoff wavelengths for each size of the modulator are indicated by the vertical dotted line in the figure. Extinction ratio becomes large when wavelength increases, but decreases rapidly near the cutoff wavelength λ_{cut}. This can be explained as follows. The propagation loss α becomes large when wavelength increases, as

shown in Fig. 12(a), because the penetration depth of the evanescent wave into the polysilicon layer becomes large, as shown in Fig. 12(b). However, the propagation losses $\alpha(V_G)$, $\alpha(0)$, and $|\alpha(V_G) - \alpha(0)|$ decrease rapidly in the limit $\lambda \rightarrow \lambda_{cut}$ [19, 20] because L_{xpq} in eq. (7) increases rapidly. Figure 11(d) also shows that the free-carrier-absorption-based modulator is insensitive to wavelength compared with the phase-shift-based modulator.

3.4 Absorption by surface plasmons

Since the inversion layer behaves like a metal film, it is expected that the guided waves interact with surface plasmons[21, 22] at the interface of the inversion layer and the gate oxide film. A surface plasmon oscillates with large amplitude when coupled with a light wave. The light coupled with the surface plasmon loses energy because part of light energy moves to the surface plasmon, and a large energy dissipates by plasma oscillation. The sharp decrease in reflectivity for the TM polarized wave in Fig. 4(c) or the large extinction ratio in Fig. 9 is caused by surface plasmons.

The optical modulation mechanism by surface plasmons is the same as that of conventional free carrier absorption shown in Fig. 2(b). However, the decrease in optical power by one reflection is very large, thus a larger extinction ratio is expected. Since the condition that surface plasmon resonance occurs depends on the thickness of the metal thin film, the incident angle of light, wavelength, and so on, it is necessary to estimate various parameters of the optical modulator.

Figure 13 shows the incident angle and gate voltage dependences of reflectivity when the TM polarized wave with λ = 1.55 μm enters the multilayer structure shown in Fig. 4 (a) with a 5-nm-thick gate oxide film. A decrease in reflectivity by surface plasmons appears when the gate voltage is approximately 6.1 V. In the proposed modulator, absorption by surface plasmons is not very large because the inversion layer is very thin (10 nm or less). Figure 14 shows the gate voltage dependence

of extinction ratio for the E_{11}^{y} mode of the proposed modulator with T_{core} = 1.5 μm, W_{core} = 2 μm, and z = 5 mm (a), and T_{core} = W_{core} = 0.5 μm and z = 5 mm (b). Very large extinction ratios are obtained, which were further increased by reducing the size of the waveguide. However, a strong coupling between guided modes and surface plasmons does not occur when gate voltage is not applied beyond the dielectric breakdown of the gate oxide film. Thus, it is necessary to use a high-k material, for example, HfO_2, as a gate insulating film in order to realize a surface-plasmon-based modulator in the 1.55-μm-wavelength regime.

Figure 15 shows the wavelength dependence of propagation loss for the E_{11}^{y} mode of the proposed modulator with T_{core} = 1.5 μm, W_{core} = 2 μm, and z = 5 mm, and the 5-nm-thick gate oxide film. The curve denotes the cases of applying gate voltages V_G = 3, 4, 5, and 5.9 V (dielectric breakdown voltage is about 5.9 V). For example, a large attenuation by surface plasmons appears at approximately 3.8 μm when a gate voltage of 3 V is applied. It is difficult to obtain a large propagation loss by surface plasmons at a wavelength of 1.55 μm owing to the gate oxide breakdown. However, in the case of a longer wavelength, large extinction ratios are obtained at a lower gate voltage.

4. Conclusions

The potentiality of the MOS optical modulator based on free carrier absorption is discussed theoretically utilizing Marcatili's approximation. The extinction ratio in the 1.55-μm-wavelength regime is limited at 1 dB owing to the limited interaction between light and free carriers. Even though the response is very small, the free carrier absorption of the proposed device is confirmed by theoretical analysis as well as experimental results reported in ref. 8.

In the deeper infrared regime, it is expected that an extinction ratio of approximately 8 dB is obtained in the case of a 1.5-μm-thick waveguide. However, the theoretical result is restricted at a

wavelength smaller than 9 μm because of the large extinction coefficient of SiO_2[18].

A much larger extinction ratio is expected when guided waves and surface plasmons interact. In the case of the wavelength λ = 1.55 μm, it is difficult to obtain the absorption by surface plasmons owing to the dielectric breakdown of the gate oxide film. However, in the case of a longer wavelength, the large absorption by surface plasmons is expected at a lower gate voltage.

One of the advantages of this modulator is that the guided mode need not be taken into consideration, that is, whether single mode or multimode. The extinction ratio of the higher-order mode is larger than that of the fundamental mode because the propagation loss of the higher-order mode is larger than that of the fundamental mode. Thus, this device has a possible application as a modulator even with the multimode propagation.

1) G. V. Treyz, Paul G. May, and Jean-Marc Halbout: IEEE Electron Device Lett. **12** (1991) 276.

2) A. Liu, R. Jones, L. Liao, D. Samara-Rubio, D. Rubin, O. Cohen, R. Nicolaescu, and M. Panicca: Nature **427** (2004) 615.

3) L. Liao, D. Samara-Rubio, A. Liu, D. Rubin, U. D. Keil, T. Franck, D. Hodge, and M. Panicca: Jpn. J. Appl. Phys. **45** (2006) 6603.

4) L. Liao, A. Liu, D. Rubin, J. Basak, Y. Chetrit, H. Nguyen, R. Cohen, N. Izhaky, and M. Paniccia: Electron. Lett. **43** (2007) 1196.

5) A. Sciuto, S. Libertino, S. Coffa, and G. Coppola: Appl. Phys. Lett. **86** (2005) 201115.

6) Q. Xu, B. Schmidt, S. Pradhan, and M. Lipson: Nature **435** (2005) 325.

7) T. Furukawa and H. Sunami: Ext. Abstr. (61st Autumn Meet., 2000); Japan Society of Applied Physics and Related Societies, 6p-ZK-1, p. 94 [in Japanese].

8) T. Hirata, K. Kajikawa, T. Tabei, and H. Sunami: Jpn. J. Appl. Phys. **47** (2008) 2906.

9) T. Tabei, T. Hirata, K. Kajikawa, and H. Sunami: IEDM Tech. Dig., 2007, p. 1023.

10) W. Spitzer and H. Y. Fan: Phys. Rev. **108** (1957) 268.

11) P. E. Schmid: Phys. Rev. B **23** (1981) 5531.

12) R. A. Soref and J. P. Lorenzo: IEEE J. Quantum. Electron. **22** (1986) 873.

13) S. M. Sze: *Physics of Semiconductor Devices* (Wiley, New York, 1981) 2nd ed., p. 29.

14) E. Barta: Infrared Phys. **17** (1977) 111.

15) Y. Taur and T. H. Ning: *Fundamentals of Modern VLSI Devices* (Cambridge University Press, New York, 1998) p. 133.

16) J. Homola: in *Surface Plasmon Resonance Based Sensors*, ed. J. Homola (Springer, Berlin, 2006) p. 3.

17) E. A. J. Marcatili: Bell Syst. Tech. J. **48** (1969) 2071.

18) H. R. Philipp: in *Handbook of Optical Constants of Solids*, ed. E. D. Palik (Academic Press, New York, 1985) p. 749.

19) J. Xiaoqing, Y. Jianyi, and W. Mingghua: Opt. Commun. **129** (1996) 173.

20) S. X. She: Opt. Commun. **135** (1997) 241.

21) J. Homola, J. Čtyroký, M. Skalský, J. Hradilová, and P. Kolářová: Sens. Actuators B **38-39** (1997) 286.

22) J. A. Dionne, L. A. Sweatlock, and H. A. Atwater: Phys. Rev. B **72** (2005) 075405.

Figure captions

Fig. 1. Wavelength dependence of absorption coefficient of (a) boron- and (b) phosphorus-doped crystalline silicon calculated using eq. (1). N_A and N_D denote impurity concentrations.

Fig. 2. Structure of proposed silicon optical modulator (a) and model of light propagation in SOI (b). An inversion layer appears when a large bias voltage is applied.

Fig. 3. Real part of dielectric function Re(ε) and the absorption coefficient of the inversion layer with applied gate voltage. t_{ox} denotes the thickness of the thin SiO_2 film.

Fig. 4. Reflectivity of TE and TM polarized plane waves entering from SOI to multilayer. The sharp decrease observed for TM polarized waves is due to absorption by surface plasmons.

Fig. 5. Cross section of the waveguide under study and analytical region of Marcatili's method in which the shaded regions are ignored. Relatively very thin SiO_2 layers are ignored for simplicity.

Fig. 6. Field distribution plot of guided modes E_{11}^{y}, E_{21}^{y}, and E_{31}^{y} obtained by Marcatili's approximation with simplified structure shown in Fig. 5.

Fig. 7. Parameter setting in eqs. (7)-(9). In the case of the E_{11}^{y} mode, reflection occurs as TE polarized on S_1 and S_2, and TM polarized on S_3 and S_4.

Fig. 8. Gate voltage dependence of propagation loss (a) and extinction ratio (b) of E_{11}^{y} mode for the proposed optical modulator. The waveguide size is fixed as T_{core} = 1.5 μm, W_{core} = 50 μm, and modulation length z = 5 mm.

Fig. 9. Gate voltage dependence of propagation loss (a) and extinction ratio (b) of E_{11}^{x} mode for the proposed modulator. The waveguide size is T_{core} = 1.5 μm, W_{core} = 50 μm, and z = 5 mm.

Fig. 10. Optical responses of the fabricated device reported in ref. 8 and theoretical plot including high-order mode calculated in this work. P_{on} is set to the value at a gate voltage of -1 V.

Fig. 11. Gate voltage dependence of extinction ratio for wavelengths λ = 3 μm (a) and λ = 5 μm (b), wavelength dependence of refractive index of Si and SiO_2 (c), and wavelength dependence of extinction ratio (d). Vertical dotted lines denote cutoff wavelengths for each size of waveguide.

Fig. 12. (a) Propagation loss vs wavelength λ, which is normalized by core thickness T_{core}. For T_{core} = 1.5 μm, calculation is terminated at λ = 9 μm. (b) Field distribution plot of E_{11}^{y} mode for various wavelengths, and wavelength dependence of penetration depth.

Fig. 13 Incident angle and gate voltage dependences of reflectivity when the TM polarized wave with λ = 1.55 μm enters the multilayer structure shown in Fig. 4(a) with 5-nm-thick gate oxide film.

Fig. 14 Gate voltage dependence of extinction ratio of E_{11}^{y} mode for optical modulator with T_{core} = 1.5 μm, W_{core} = 2 μm (a), T_{core} = W_{core} = 0.5 μm, and z = 5 mm (b) when wavelength λ = 1.55 μm.

Fig. 15. Wavelength dependence of the propagation loss of E_{11}^{y} mode for optical modulator with T_{core} = 1.5 μm, W_{core} = 2 μm, and t_{ox} = 5nm.

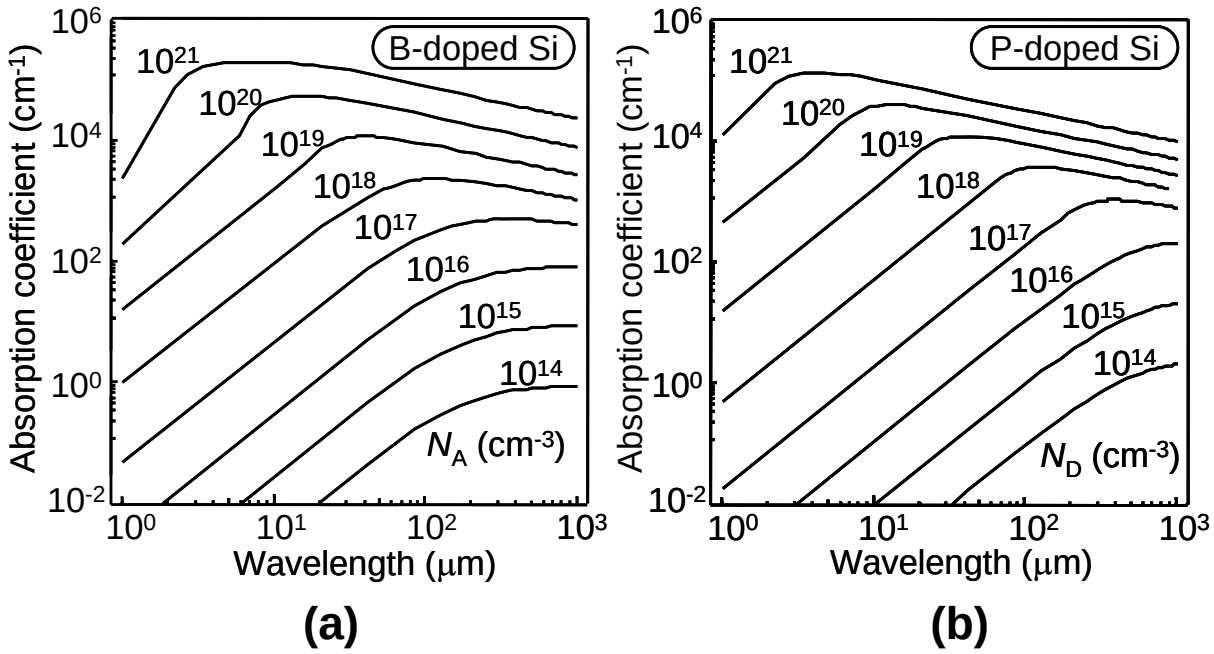
B-doped Si
10^{21}
10^{20}
10^{19}
10^{18}
10^{17}
10^{16}
10^{15}
10^{14}
N_A (cm^{-3})
Absorption coefficient (cm^{-1})
Wavelength (μm)
(a)
P-doped Si
N_D (cm^{-3})
(b)

Fig. 1

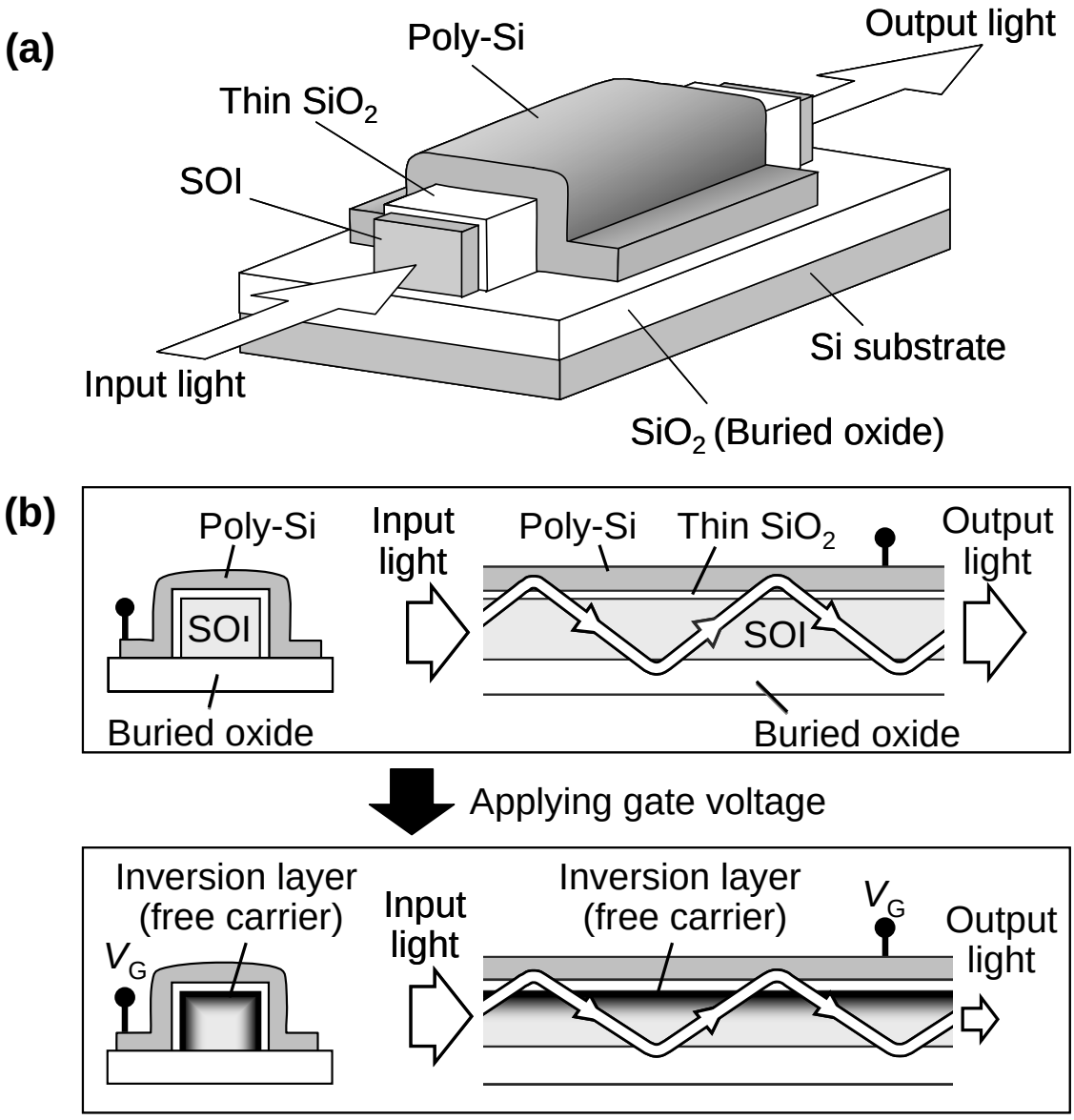
(a)
Poly-Si
Output light
Thin SiO2
SOI
Input light
Si substrate
SiO2 (Buried oxide)
(b)
Poly-Si
Input light
Poly-Si
Thin SiO2
Output light
SOI
SOI
Buried oxide
Buried oxide
Applying gate voltage
Inversion layer (free carrier)
VG
Input light
Inversion layer (free carrier)
VG
Output light

Fig. 2

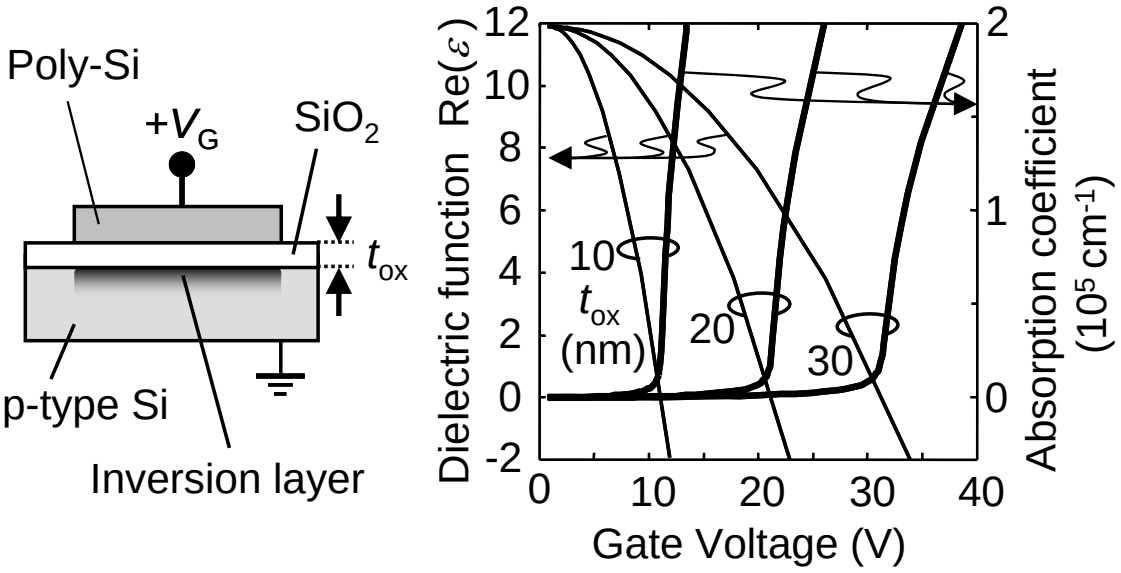
Poly-Si
+V_G
SiO_2
t_{ox}
p-type Si
Inversion layer
Dielectric function Re(ε)
Absorption coefficient (10^5 cm^{-1})
Gate Voltage (V)
10
20
30
t_{ox} (nm)

Fig. 3

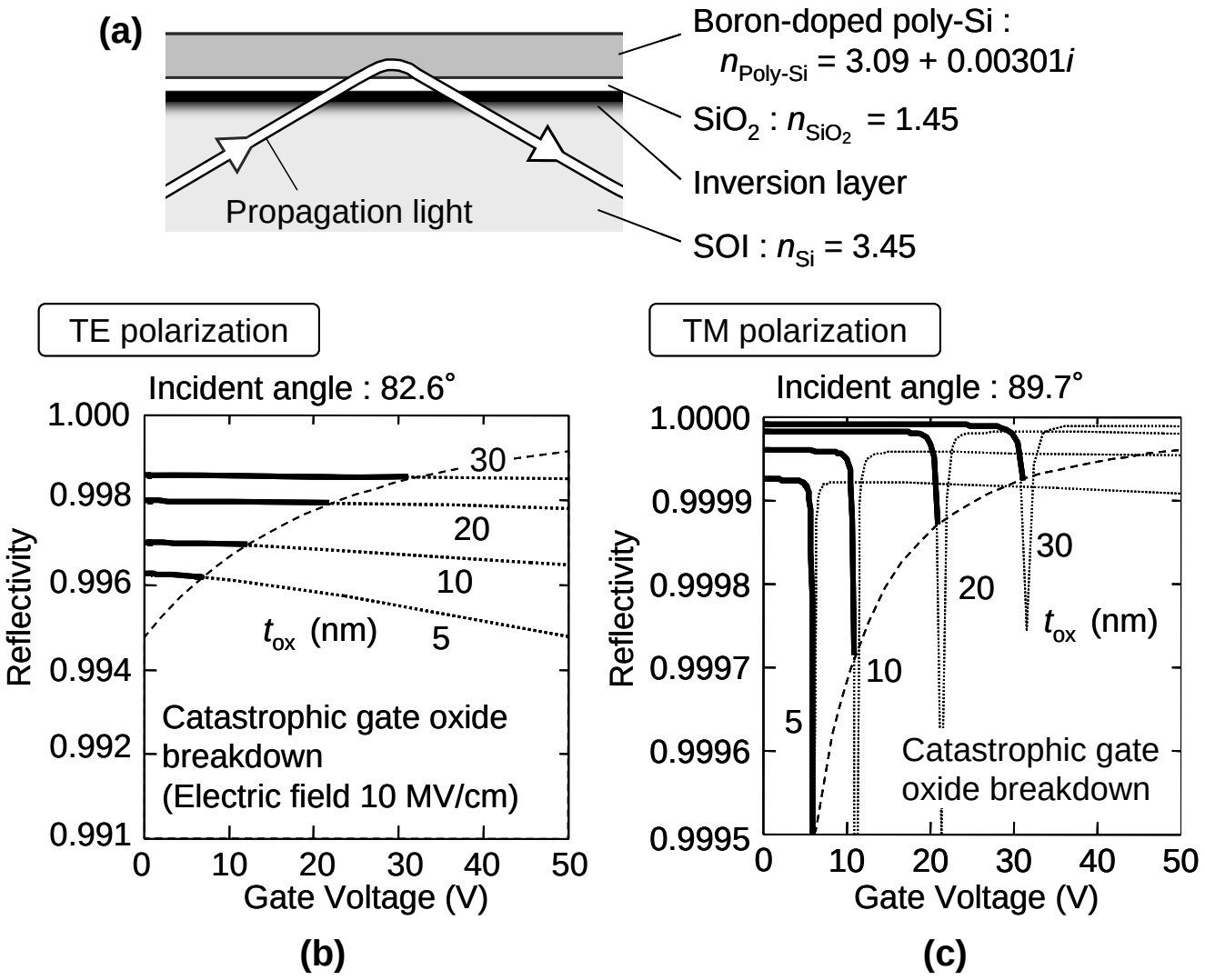
(a)
Boron-doped poly-Si :
$n_{Poly-Si}$ = 3.09 + 0.00301i
SiO_2 : n_{SiO_2} = 1.45
Inversion layer
SOI : n_{Si} = 3.45
Propagation light
TE polarization
Incident angle : 82.6˚
Reflectivity
1.000
0.998
0.996
0.994
0.992
0.991
30
20
10
5
t_{ox} (nm)
Catastrophic gate oxide breakdown
(Electric field 10 MV/cm)
0
10
20
30
40
50
Gate Voltage (V)
(b)
TM polarization
Incident angle : 89.7˚
Reflectivity
1.0000
0.9999
0.9998
0.9997
0.9996
0.9995
30
20
10
5
t_{ox} (nm)
Catastrophic gate oxide breakdown
0
10
20
30
40
50
Gate Voltage (V)
(c)

Fig. 4

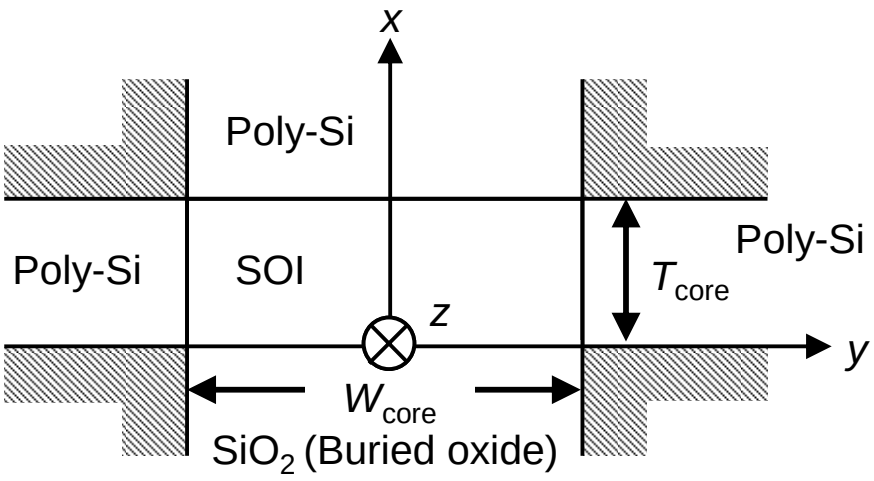

Fig. 5

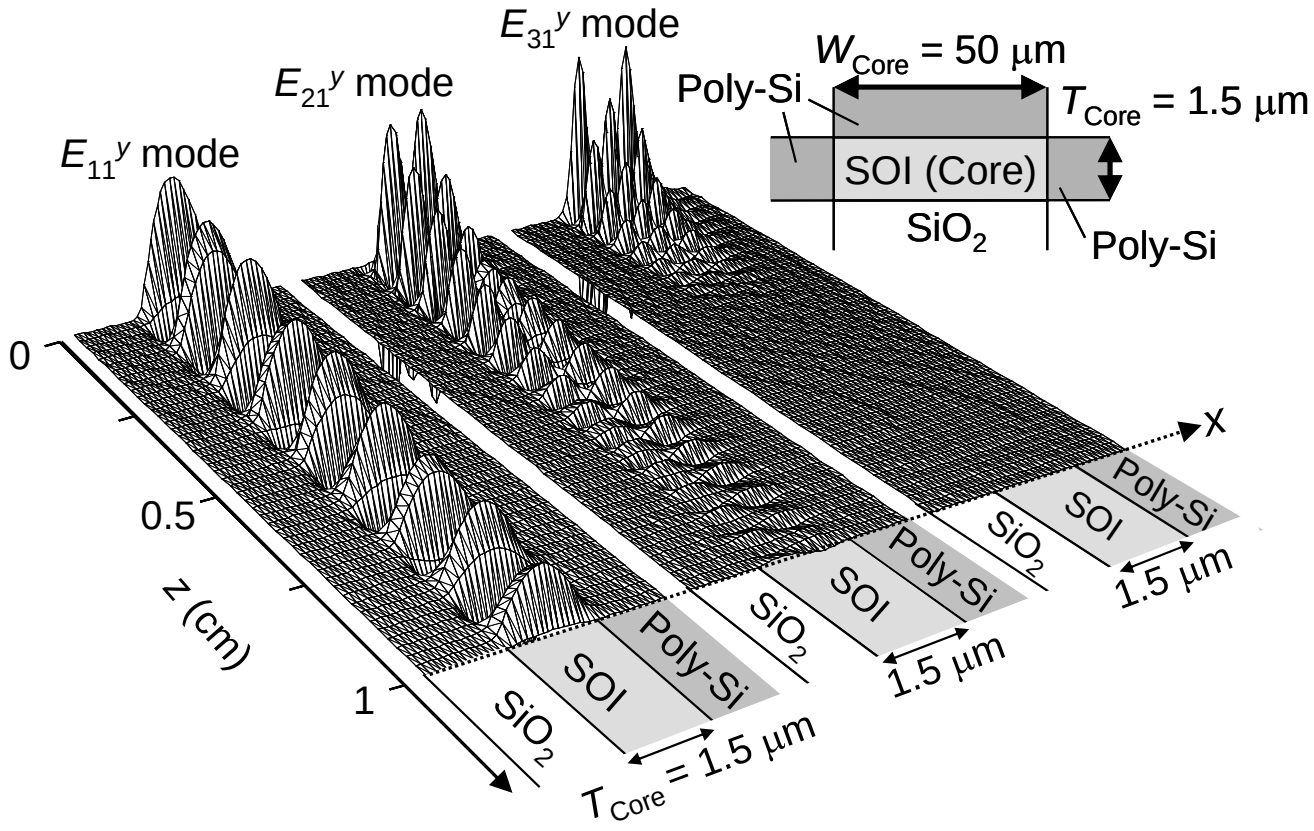
E_{31}^{y} mode
E_{21}^{y} mode
E_{11}^{y} mode
W_{Core} = 50 μm
Poly-Si
T_{Core} = 1.5 μm
SOI (Core)
SiO_2
Poly-Si
0
0.5
1
z (cm)
x
Poly-Si
SOI
SiO_2
1.5 μm
T_{Core} = 1.5 μm

Fig. 6

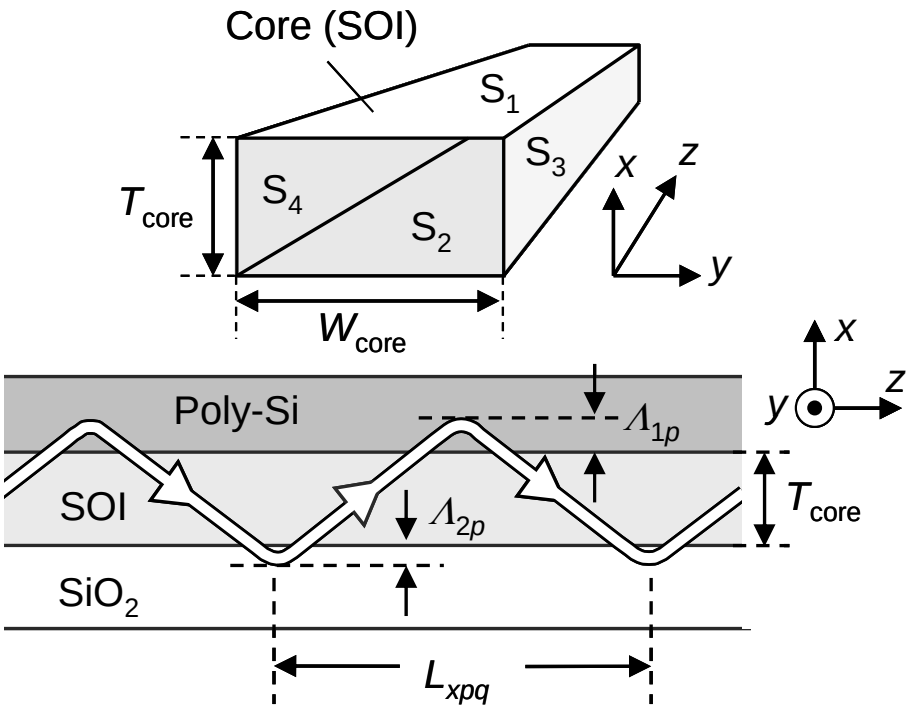
Core (SOI)
S1
S3
S4
S2
Tcore
Wcore
x
z
y
Poly-Si
SOI
SiO2
Λ1p
Λ2p
Tcore
Lxpq

Fig. 7

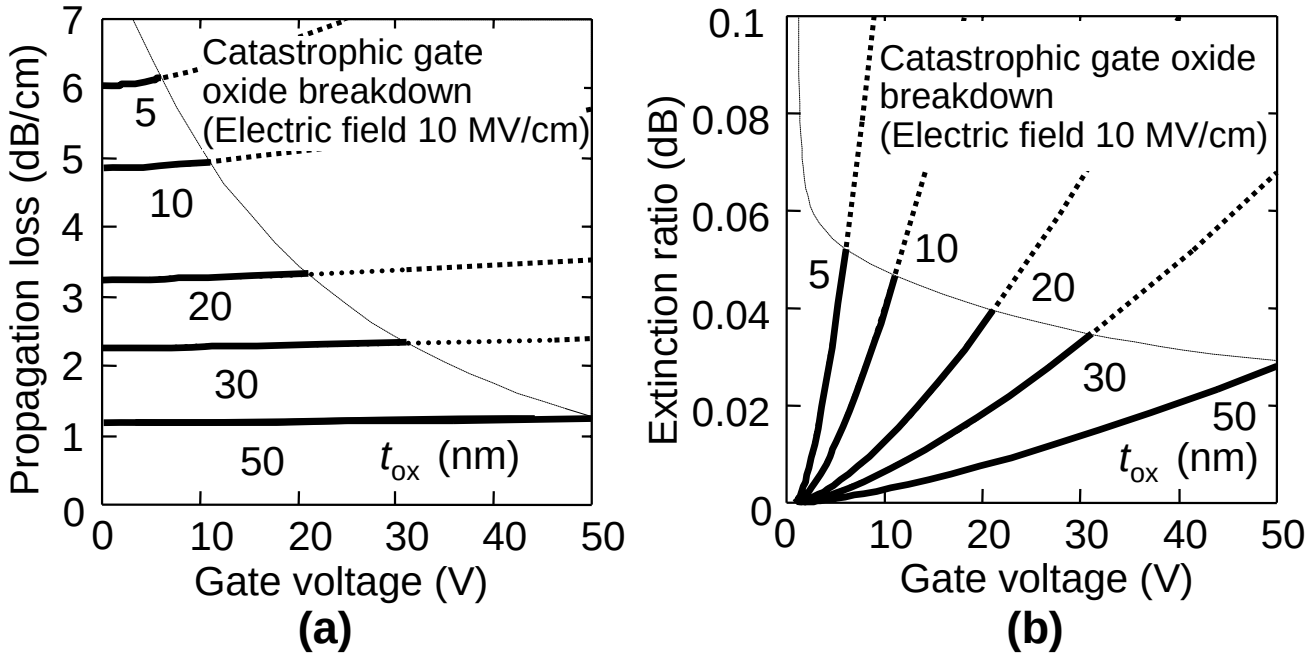
Propagation loss (dB/cm)
Catastrophic gate oxide breakdown (Electric field 10 MV/cm)
5
10
20
30
50
t_{ox} (nm)
Gate voltage (V)
(a)
Extinction ratio (dB)
Catastrophic gate oxide breakdown (Electric field 10 MV/cm)
5
10
20
30
50
t_{ox} (nm)
Gate voltage (V)
(b)

Fig. 8

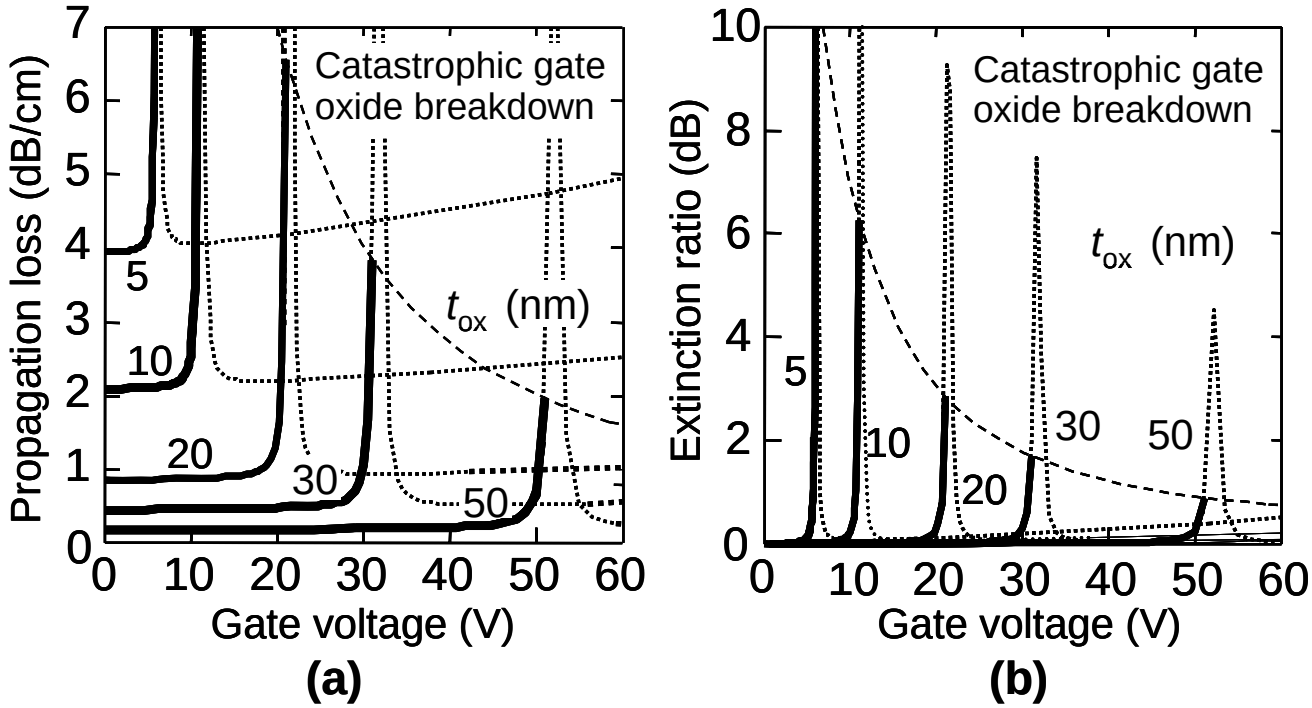
Propagation loss (dB/cm)
Gate voltage (V)
Catastrophic gate oxide breakdown
t_{ox} (nm)
5
10
20
30
50
(a)
Extinction ratio (dB)
Gate voltage (V)
Catastrophic gate oxide breakdown
t_{ox} (nm)
5
10
20
30
50
(b)

Fig. 9

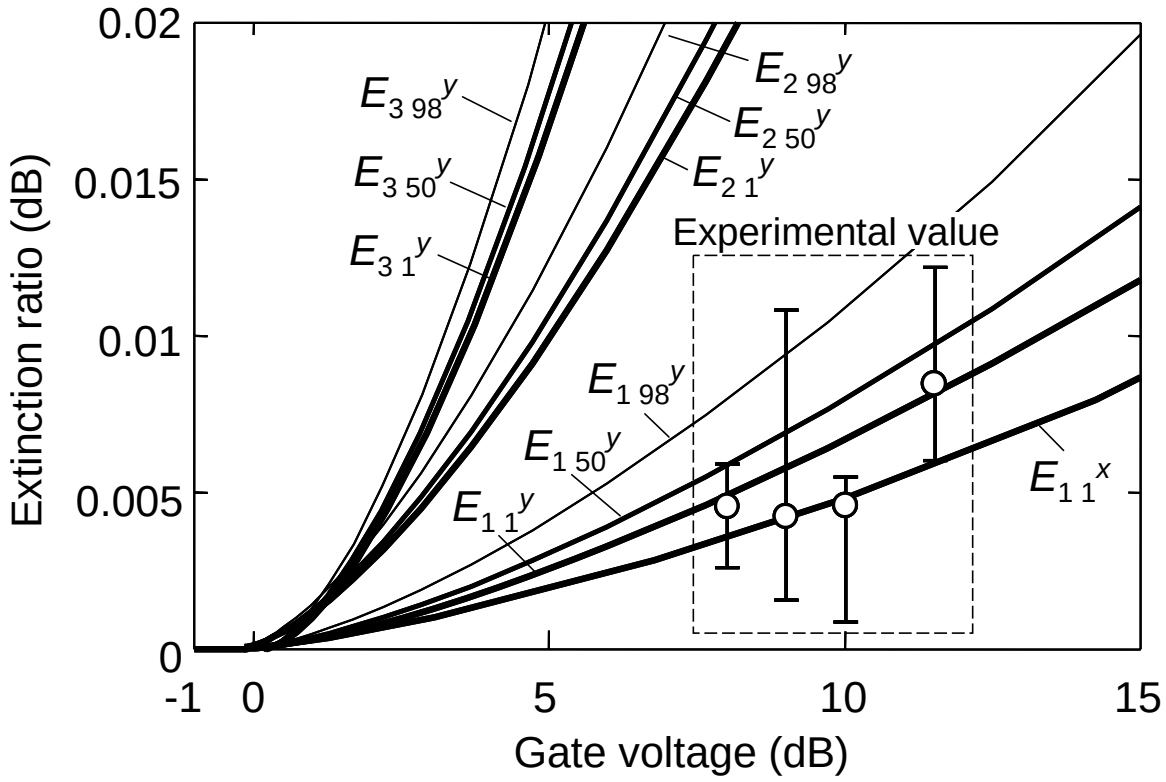
0.02
0.015
0.01
0.005
0
Extinction ratio (dB)
-1
0
5
10
15
Gate voltage (dB)
$E_{3\,98}^{y}$
$E_{3\,50}^{y}$
$E_{3\,1}^{y}$
$E_{2\,98}^{y}$
$E_{2\,50}^{y}$
$E_{2\,1}^{y}$
Experimental value
$E_{1\,98}^{y}$
$E_{1\,50}^{y}$
$E_{1\,1}^{y}$
$E_{1\,1}^{x}$

Fig. 10

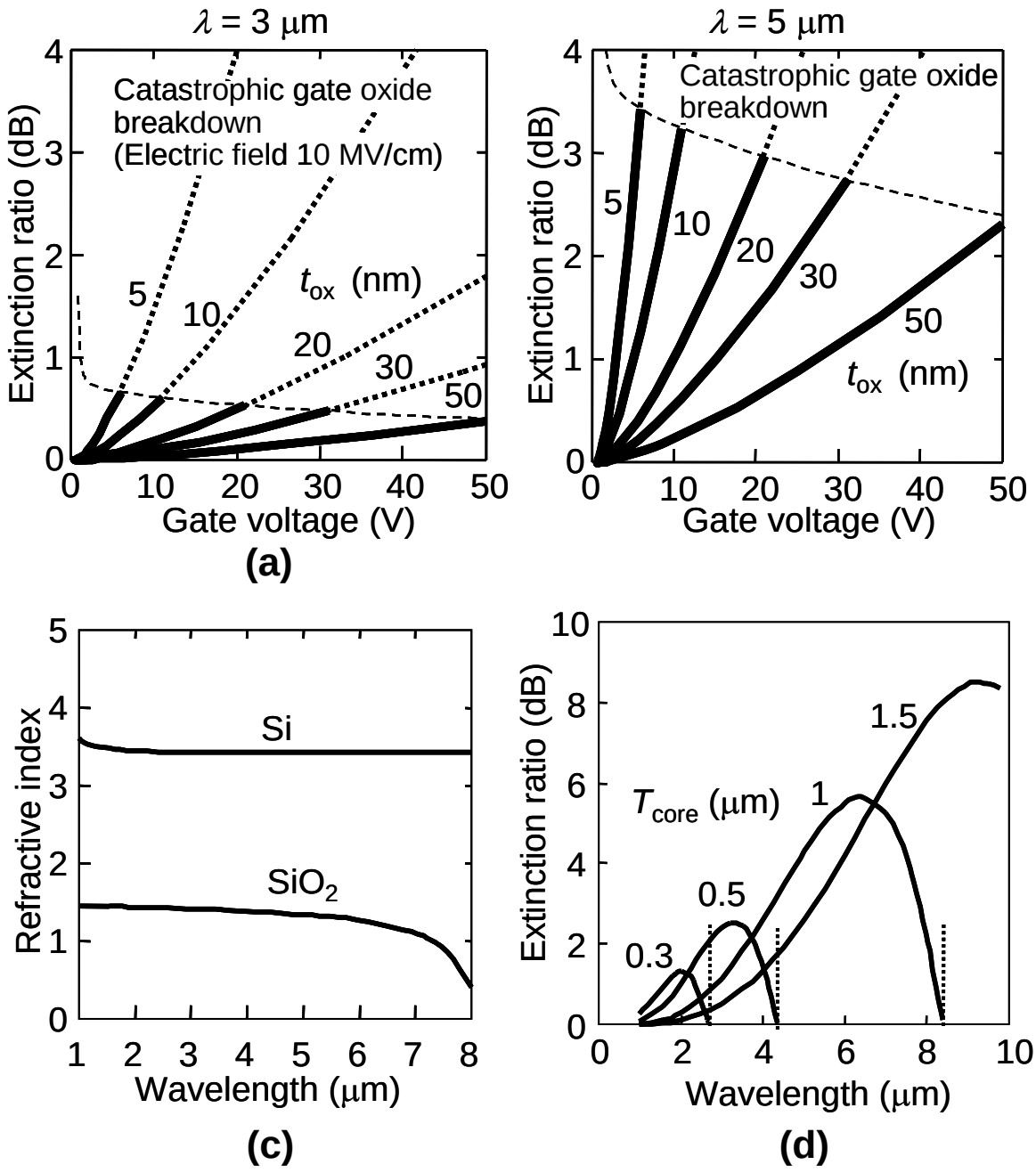
λ = 3 μm
Catastrophic gate oxide breakdown
(Electric field 10 MV/cm)
Extinction ratio (dB)
Gate voltage (V)
5
10
20
30
50
t_{ox} (nm)
(a)
λ = 5 μm
Catastrophic gate oxide breakdown
Extinction ratio (dB)
Gate voltage (V)
5
10
20
30
50
t_{ox} (nm)
Refractive index
Si
SiO_2
Wavelength (μm)
(c)
Extinction ratio (dB)
T_{core} (μm)
0.3
0.5
1
1.5
Wavelength (μm)
(d)

Fig. 11

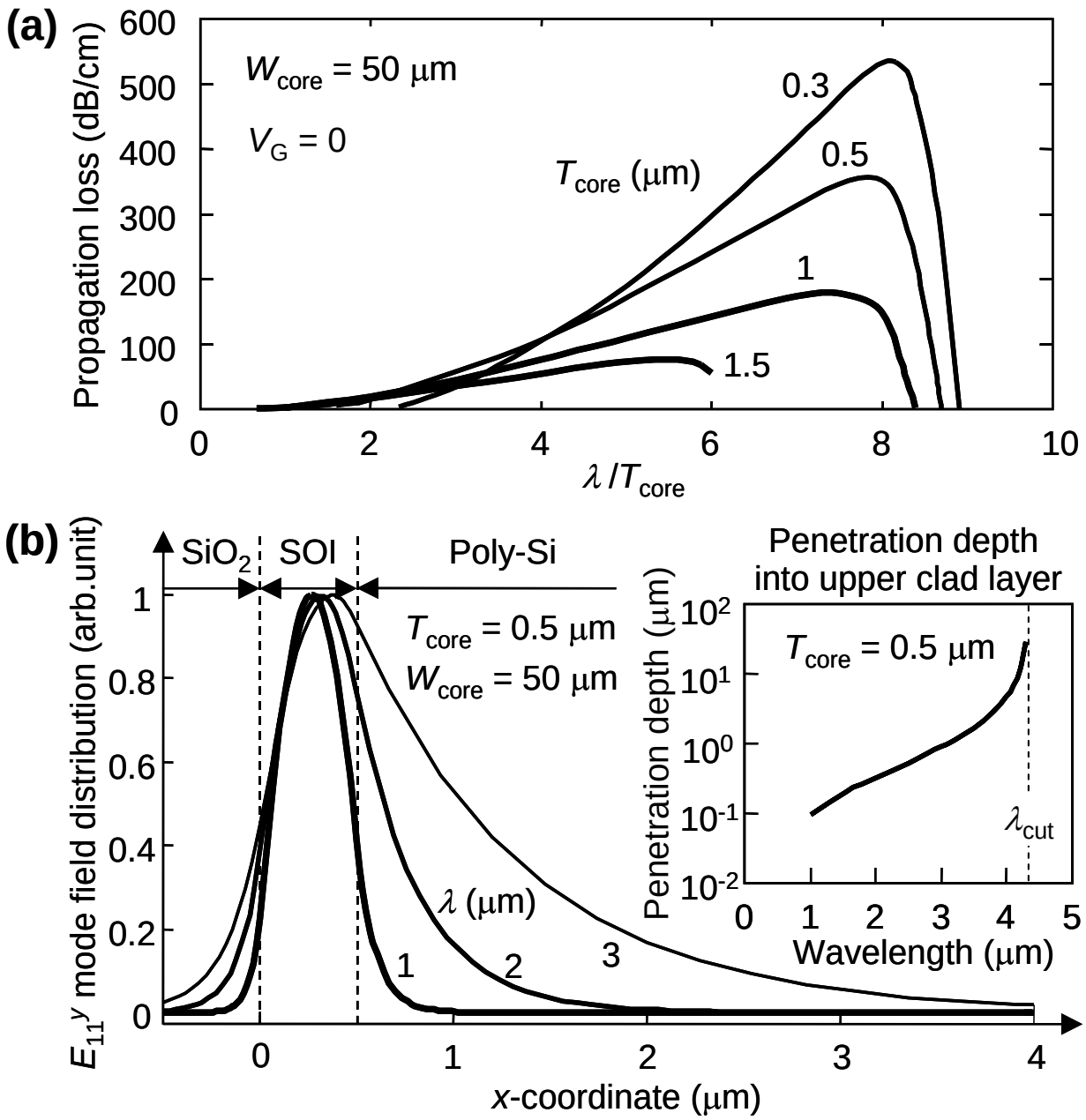
(a)
Propagation loss (dB/cm)
600
500
400
300
200
100
0
W_{core} = 50 μm
V_G = 0
T_{core} (μm)
0.3
0.5
1
1.5
0
2
4
6
8
10
λ /T_{core}
(b)
SiO_2
SOI
Poly-Si
T_{core} = 0.5 μm
W_{core} = 50 μm
λ (μm)
1
2
3
E_{11}^y mode field distribution (arb.unit)
1
0.8
0.6
0.4
0.2
0
0
1
2
3
4
x-coordinate (μm)
Penetration depth into upper clad layer
Penetration depth (μm)
10^2
10^1
10^0
10^{-1}
10^{-2}
T_{core} = 0.5 μm
λ_{cut}
0
1
2
3
4
5
Wavelength (μm)

Fig. 12

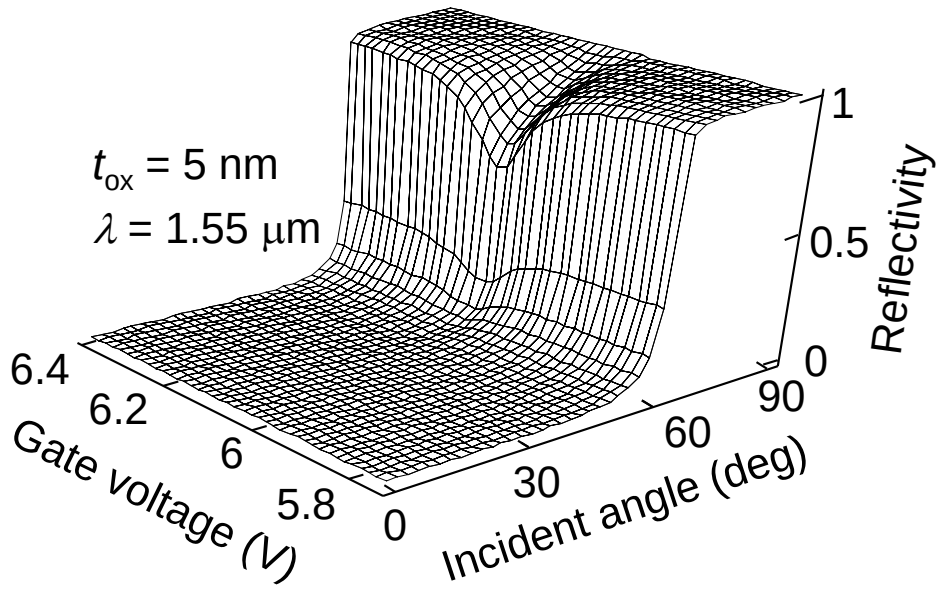
t_{ox} = 5 nm
λ = 1.55 μm
6.4
6.2
6
5.8
Gate voltage (V)
0
30
60
90
Incident angle (deg)
1
0.5
0
Reflectivity

Fig. 13

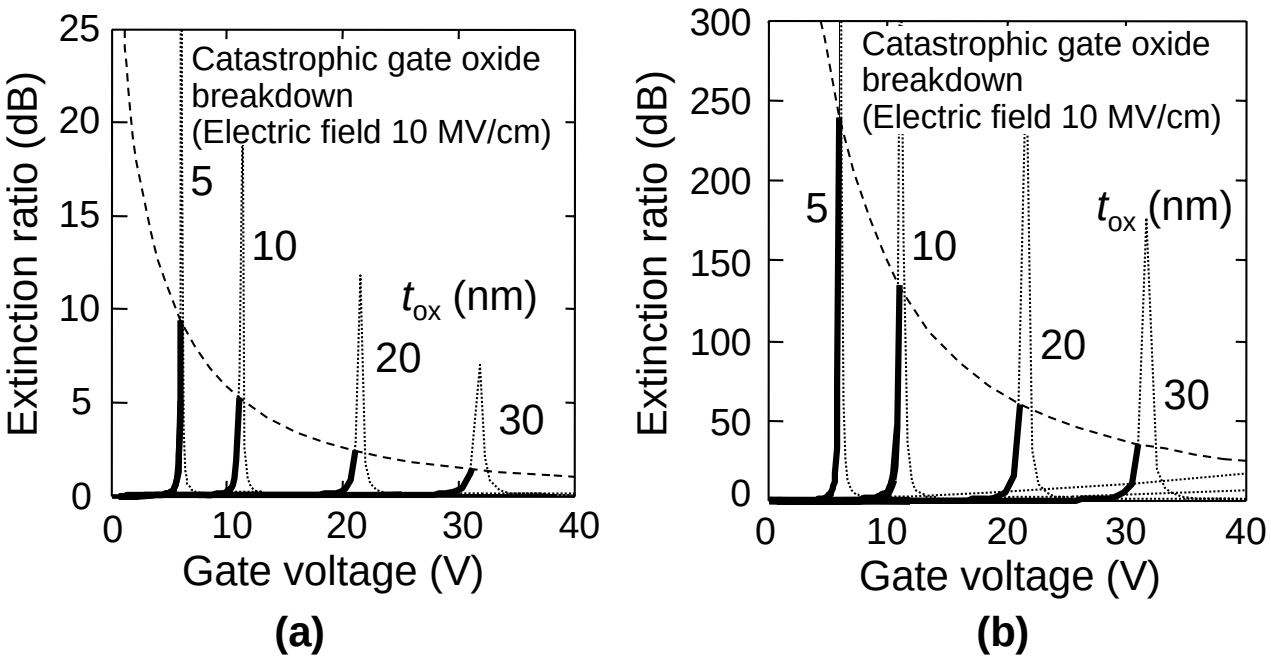
Extinction ratio (dB)
Gate voltage (V)
Catastrophic gate oxide breakdown
(Electric field 10 MV/cm)
5
10
20
30
t_{ox} (nm)
(a)
(b)

Fig. 14

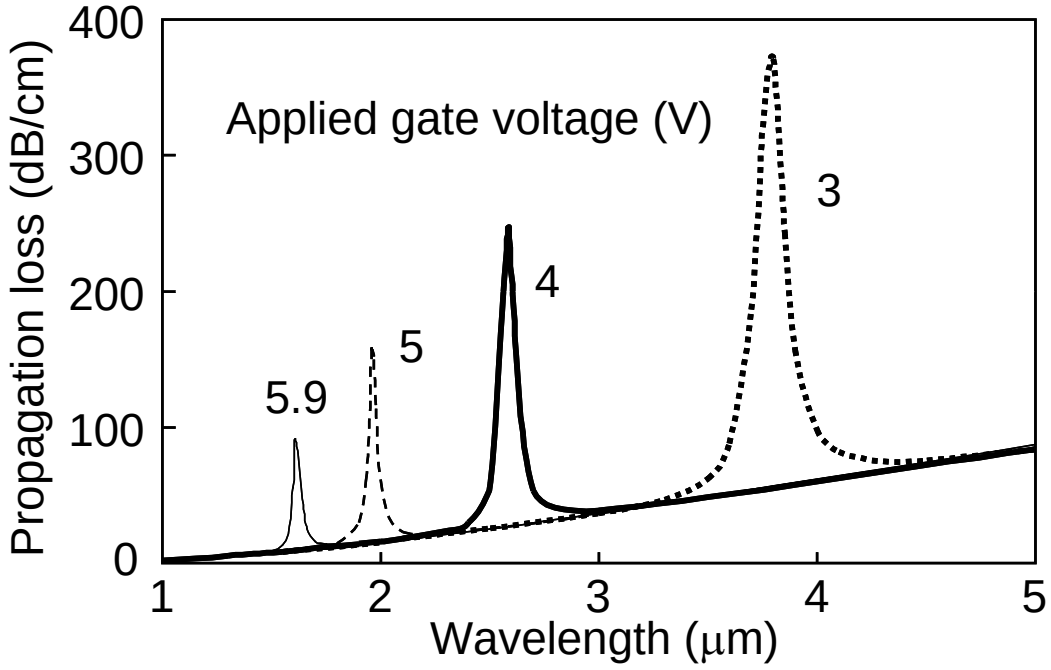
Propagation loss (dB/cm)
400
300
200
100
0
1
2
3
4
5
Wavelength (μm)
Applied gate voltage (V)
5.9
5
4
3

Fig. 15